Magnetotransport through semiconductor superlattices

F. Elsholz, A. Wacker, and E. Schöll
Institute for Theoretical Physics, Technical University of Berlin, Hardenbergstrasse 36, D-10623 Berlin, Germany

M. Kast, G. Strasser, and E. Gornik
Intitute for Solid State Electronics, Technical University of Vienna, A-1040 Wien, Austria

(Received 13 September 2000; published 2 January 2001)

In this paper, we investigate transmission through short superlattices in a perpendicular magnetic field. The shift in energy of the transmission peak can be qualitatively understood in terms of the semiclassical motion in the drift region, whereas full quantitative agreement can be obtained from a quantum mechanical transport model. Interface roughness does not influence this behavior crucially.

DOI: 10.1103/PhysRevB.63.033312 PACS number(s): 73.61.−r

I. INTRODUCTION

Electronic transport in semiconductor superlattices, as first considered by Esaki and Tsu,[1] has been studied extensively using several experimental techniques as current-voltage measurements,[2] ultra short time techniques,[3] or ballistic electron spectroscopy.[4] Vertical miniband transport under dc bias conditions demonstrated the controlled decrease of superlattice conductance with increasing bias, which results from the formation of localized Wannier Stark states.[5] The asymmetric transport behavior with respect to reversal of the electric field was related to the presence of interface roughness violating the conservation of lateral momentum of the electron motion.[6] A different possibility to interchange vertical and lateral momentum is the application of a magnetic field perpendicular to the transport direction, which is studied in this work. Although transport in a *parallel* magnetic field has been measured by several groups,[7–10] the topic of a *perpendicular* magnetic field has not drawn as much attention.[11,12]

II. EXPERIMENTAL DATA

A Three-Terminal Device[6] is used to probe the transmission of an undoped $Al_{0.3}Ga_{0.7}As$ superlattice (SL). The structure, which is shown in Fig. 1, was grown by molecular beam epitaxy. An electron beam of tunable energy is generated by injection through a tunneling barrier. It passes the SL after traversing a thin highly doped n-GaAs base layer and an undoped drift region. The static transfer ratio ($=I_c/I_e$) reflects the probability of an injected electron to be transmitted through the SL. The superlattice consists of five periods of 2.5 nm $Al_{0.3}Ga_{0.7}As$ barriers and 6.5 nm GaAs wells. For these parameters a simple Kronig-Penney calculation gives the first miniband lying between 46 and 68 meV and a second one between 182 and 276 meV. The devices are fabricated by standard photolithographic and wet etching techniques. The emitter, base, and collector were contacted by a standard alloy of evaporated AuGe/Ni. In order to avoid effects of undesired electric fields at the SL, we set the base and collector voltages to zero (flat band condition). The magnetic field, produced by a superconducting magnet, was applied perpendicular to the growth direction (parallel to the superlattice layers). The emitter and collector currents were measured with a parameter analyzer at 4.2 K. Figure 2 shows a set of measured transfer ratios as a function of electron injection energy at different values of magnetic induction B. It can be seen that the peak in the transfer ratio, which is due to transport through the first miniband, shifts to higher energies with increasing B. As shown in Fig. 3, the position of the maxima can be fitted by a quadratic expression

$$\Delta E_{\max}(B) := E_{\max}(B) - E_{\max}(0) \approx c \cdot B^2, \tag{1}$$

with $c_{\exp} \approx 40$ meV/T^2. In the inset of Fig. 2 the transmission function is shown over a wider range of energies. For $B=0$ further transmission peaks at energies $E_{\max,i} \approx E_{\max} + i36$ meV are found, which can be identified as optical phonon replica. The position of these replica hardly shift with magnetic field. Nevertheless, the situation is difficult to analyze due to the interference with the shifted lowest peak.

III. THE MODEL

We denote the transport direction z (which is the growth direction) as *vertical* using the subscript $\parallel$, whereas the other directions x,y (in which the magnetic field is directed) are called *lateral*, labeled by $\perp$. Hot electrons of given energy E, charge $e<0$, and initial vertical velocity $v_\parallel(t=0)$ are generated via the tunneling injection barrier structure and reach

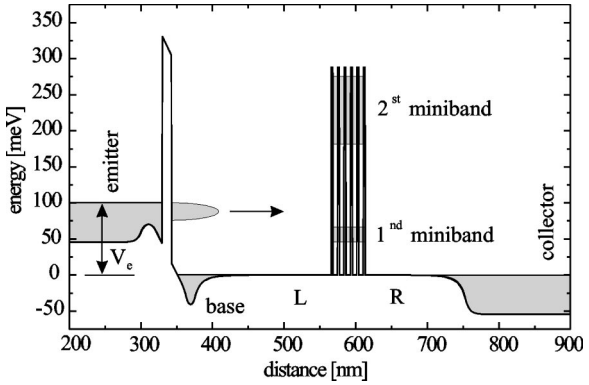

FIG. 1. Conduction band diagram of the semiconductor structure along the growth direction without external fields. The positions of the two lowest minibands are indicated by shaded areas.

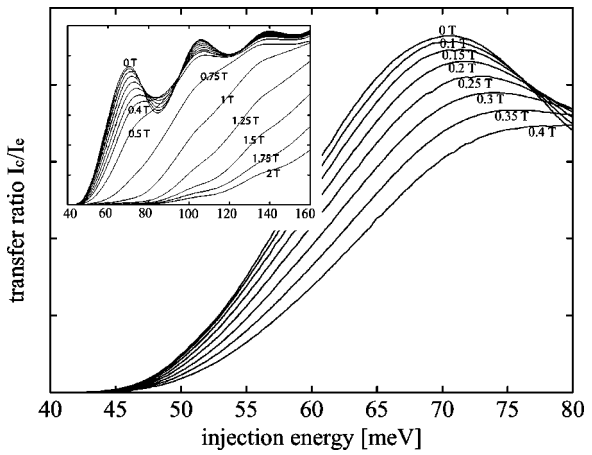

FIG. 2. Measured transfer ratio through the first miniband of a five period $Al_{0.3}Ga_{0.7}As$ SL vs injection energy for different magnetic fields. The inset shows the data for larger injection energies, where phonon replica of the first peaks can be observed.

the superlattice after traversing ballistically the drift region of length l. In this quasi-unconfined region, electron motion is assumed to be semiclassical and described by the well-known trajectory with effective mass m^*, which leads to a nonvertical impact onto the SL due to the external magnetic field. As long as the magnetic field $\mathbf{B}=B\mathbf{e}_y$ is weak enough for the electrons to reach the SL, the lateral component of the velocity at the time of impact τ is found from the semiclassical equations of motion to be

$$v_\perp = \int_0^\tau \frac{|e|v_\parallel(t)B}{m^*}dt = \frac{|e|lB}{m^*} \tag{2}$$

carrying a lateral energy

$$E_\perp = \frac{e^2l^2B^2}{2m^*}. \tag{3}$$

This energy has to be subtracted from the kinetic energy in the growth direction which determines the transmission probabilities. This yields Eq. (1) with the constant $c_{\mathrm{class}} = e^2l^2/(2m^*) = 52.5\ \mathrm{meV/T^2}$ for $l=200$ nm and $m^* = 0.067m_e$ as indicated in Fig. 3. Though this procedure gives qualitative agreement with the quadratic shift observed experimentally, the obtained value of c_{class} is too large compared to the experimental result $c_{\mathrm{exp}} \simeq 40\ \mathrm{meV/T^2}$.

The discrepancy can be overcome by considering the transmission through the SL quantum mechanically. The field-free case is formulated in terms of the equilibrium Green's function $G^{\mathrm{Ret}}(E)$ at given *total* energy E defined by[13]

$$\left(E - \hat{H} - \sum_{\alpha,\mathbf{k}} \Sigma^{\mathrm{Ret}}_{\alpha,\mathbf{k}}(E)\right) G^{\mathrm{Ret}}(E) = \mathbf{1}, \tag{4}$$

where $\hat{H} = \hat{H}^0 + \hat{H}'_C$ is the Hamiltonian comprising a field-free ordered part of the SL region and a term describing interface roughness (see Ref. 14 for details). The term $\Sigma^{\mathrm{Ret}}_{\alpha,\mathbf{k}}(E)$ describes the self-energy contributions due to coupling to a lead $\alpha \in \{L,R\}$ [drift regions before (L) and after (R) the SL] and mode $\mathbf{k}$ (incident or outgoing electron waves, respectively). Using plane waves $|\mathbf{k}\rangle := e^{i\mathbf{k}\cdot\mathbf{r}}/\sqrt{A}$ as a basis in the lateral direction [$\mathbf{r}=(r_x,r_y)$ and $\mathbf{k}=(k_x,k_y)$ denote lateral, two-dimensional vectors, A is a normalization area] and Wannier states $\psi_n(z)$ of the lowest miniband localized at well n as basis funcions in growth direction, we obtain

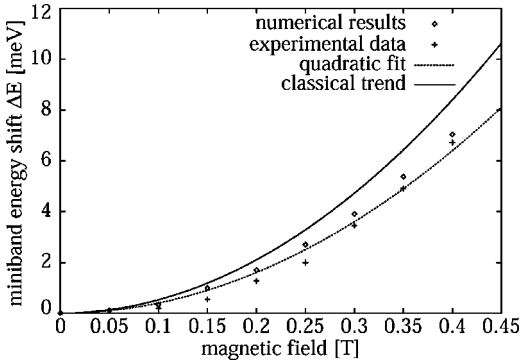

FIG. 3. Dependence of the shift in energy of the miniband center upon the magnetic field: experimental data (crosses), classical behavior with $c_{\mathrm{class}} = 52.5\ \mathrm{meV/T^2}$ (solid line), quantum mechanical calculation (squares), and a quadratic fit with $c_{\mathrm{exp}} = 40\ \mathrm{meV/T^2}$ (dotted line).

$$H^0_{n\mathbf{k},n'\mathbf{k}'} = \delta_{\mathbf{k},\mathbf{k}'}\Bigg((E_k + E^a)\,\delta_{n,n'} + \sum_{\zeta=1}^{\infty} T^a_\zeta(\,\delta_{n,n'+\zeta} + \delta_{n,n'-\zeta})\Bigg). \tag{5}$$

$E_k = \hbar^2k^2/2m^*$ is the lateral energy and E^a denotes the center of the lowest miniband. The hopping energies T^a_ζ are the Fourier components of the lowest miniband dispersion relation, as obtained from one dimensional Kronig-Penney calculation.[15]

In order to solve Eq. (4) numerically, we restrict ourselves to tight-binding couplings ($\zeta=1$) and discretize[16,17] the lateral direction in each well in a square lattice with lattice constant a yielding constant lateral hopping matrix elements $t_{\mathbf{l},\mathbf{l}'} = -t = -\hbar^2/2m^*a^2$ for nearest neighbors $\mathbf{l},\mathbf{l}'$ and on-site energies $U_{n,\mathbf{l}} = E^a + 4t$. Here $\mathbf{l}=(lx,ly)$ denote the discrete lattice sites of a given well. The self-energy contributions from Eq. (4) are treated in the ''wide-band'' limit[14] giving rise to constant, diagonal self-energies

$$\left[\sum_{\mathbf{k}} \Sigma^{\mathrm{Ret}}_{\alpha,\mathbf{k}}\right]_{n\mathbf{l},n'\mathbf{l}'} = -i\frac{\Gamma^\alpha}{2}\delta_{n,n_\alpha}\delta_{n',n_\alpha}\delta_{\mathbf{l},\mathbf{l}'} \tag{6}$$

for each lead α [$n_\alpha = 0$ (or $N-1$) for $\alpha = L$ (or R), respectively]. N is the number of periods, Γ^α are the self-energy constants evaluated as in Ref. 14.

Interface roughness is taken into account in the on-site energies by additive local potential fluctuations $U_{\mathrm{loc}}(n,\mathbf{l}) = A_0 \cdot \{-1,0,1\}$ corresponding to individual variations of local-well widths due to growth fluctuations of N_{ML} monolayers with $N_{\mathrm{ML}} \in \{-2,0,2\}$.[18,14]

An external magnetic field is included as follows. We

TABLE I. Numerical parameters for a superlattice with $Al_{0.3}Ga_{0.7}As$ barriers of width 2.5 nm and GaAs wells of width 6.5 nm. E^a is the center of the first miniband, T_1^a is the first-miniband hopping energy between neighboring wells, $t=\hbar^2/2m^*a^2$ is the lateral nearest-neighbor hopping energy for mesh size $a=5$ nm, and effective electron mass $m^*=0.067m_e$. Γ^α are the constant self-energies describing connection to the leads α and A_0 is an effective roughness-energy.

E^a	54.52 meV
T_1^a	5.84 meV
t	22.74 meV
Γ^α	2.07 meV
A_0	7 meV

choose a linear Landau-gauge for the vector potential $\mathbf{A}=Bz\mathbf{e}_x$ and perform a Peierls substitution[19] in the hopping energies

$$t_{\mathbf{l},\mathbf{l}'} \rightarrow t_{\mathbf{l},\mathbf{l}'} \cdot \exp\left\{ i\frac{e}{\hbar}\mathbf{A}\left(\frac{\mathbf{l}+\mathbf{l}'}{2}\right)\cdot(\mathbf{l}-\mathbf{l}')a \right\} \tag{7}$$

and analogously for the vertical couplings T_1^a.

Finally, the transmission probability from a particular mode $\mathbf{k}$ in the left contact L to the right contact R is calculated from $G^{\mathrm{Ret}}(E)$ via the Fisher-Lee relation[20]

$$T_{R\leftarrow(L,\mathbf{k})}=\sum_{\mathbf{k}'}\frac{\hbar^2\nu_{\mathbf{k}'}\nu_{\mathbf{k}}}{a^2}\left|\sum_{\mathbf{l}_j\in R}\chi^*_{\mathbf{k}'}(\mathbf{l}_j)\sum_{\mathbf{l}_i\in L}[G^{\mathrm{Ret}}]_{\mathbf{l}_j,\mathbf{l}_i}\chi_{\mathbf{k}}(\mathbf{l}_i)\right|^2 \tag{8}$$

neglecting magnetic effects in the leads.[21]

As outgoing modes we choose plane waves $\chi_{\mathbf{k}'}(\mathbf{l}_j) \propto e^{ia\mathbf{k}'\cdot\mathbf{l}_j}$ for all independent discrete $\mathbf{k}'$. The transversal mode $\chi_{\mathbf{k}}$ representing the incident electron is a plane wave with appropriate wave vector $\mathbf{k}=|e|lB/\hbar\mathbf{e}_x$ according to the lateral semiclassical electron velocity (2) at which it is injected into the superlattice.

IV. RESULTS

According to the experiment, all calculations are performed for a SL with 2.5 nm $Al_{0.3}Ga_{0.7}As$ barriers and 6.5 nm GaAs wells. The number of periods is $N=5$. Table I gives an overview of the resulting numerical parameters used in the following calculations.

Figure 4 shows the calculated miniband transmission for a SL without interface roughness for different magnetic fields. The miniband shift due to tilted impact is clearly evident. The peaks at the left- and right-hand border decrease with increasing magnetic field leading to a reduction of overall transmission as observed experimentally (Fig. 2). For given field B we define the center of the miniband

$$E_{\mathrm{center}}(B)=\frac{\int ET(E)dE}{\int T(E)dE}, \tag{9}$$

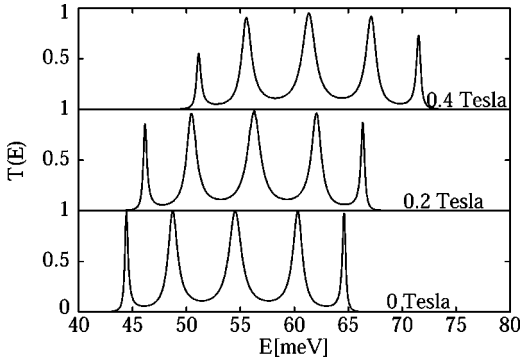

FIG. 4. Transmission probability through a five period superlattice vs energy for different perpendicular magnetic fields obtained from a three-dimensional quantum mechanical calculation.

and obtain approximately $E_{\mathrm{center}}(B)-E_{\mathrm{center}}(0)\approx c_{\mathrm{exp}}B^2$ in good quantitative agreement with the experimental result as shown in Fig. 3.

Miniband transmission including interface roughness is shown in Fig. 5 demonstrating a slight *relative* increase of the transmission peak at the right-hand border (which corresponds to the energetically highest transmission channel of the lowest miniband), while the overall transmission is broadened and reduced. This is in agreement with former theoretical results.[18] The quadratic shift of the overall transmission spectrum is not affected by interface roughness.

V. CONCLUSION

We have investigated vertical electron transport through a short superlattice with interface roughness in an external perpendicular magnetic field. The quadratic shift of the transmission peak with magnetic field can only partly be attributed to the semiclassical trajectory in the drift region. A full three-dimensional quantum mechanical calculation of the transmission through the superlattice is required for an adequate description of the experimental data. Interface rough-

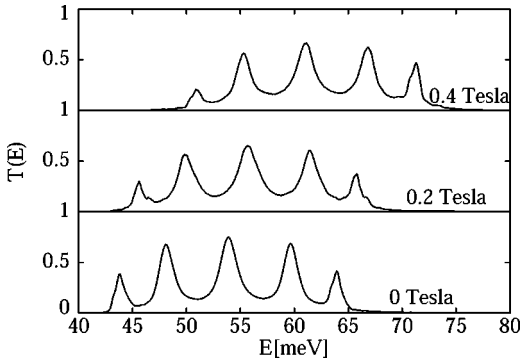

FIG. 5. Transmission probability through a five period superlattice with interface roughness vs energy for different perpendicular magnetic fields obtained from a three-dimensional quantum mechanical calculation.

ness leads to a reduction of the overall transmission probability but is of no further crucial importance. The transmission peaks due to phonon replica are less affected by the magnetic field.

ACKNOWLEDGMENTS

Helpful discussions with A. Amann, G. Kießlich, and C. Rauch are acknowledged.

[1] L. Esaki and R. Tsu, IBM J. Res. Dev. **14**, 61 (1970).
[2] *Semiconductor Superlattices, Growth and Electronic Properties*, edited by H. T. Grahn (World Scientific, Singapore, 1995).
[3] K. Leo, Physica Scripta **T68**, 78 (1996).
[4] C. H. Kuan, D. C. Tsui, and K. K. Choi, Appl. Phys. Lett. **61**, 456 (1992); P. England, J. R. Hayes, E. Colas, and M. Helm, Phys. Rev. Lett. **63**, 1708 (1989).
[5] C. Rauch, G. Strasser, K. Unterrainer, W. Boxleitner, and E. Gornik, Phys. Status Solidi B **204**, 393 (1997).
[6] C. Rauch, G. Strasser, K. Unterrainer, W. Boxleitner, E. Gornik, and A. Wacker, Phys. Rev. Lett. **81**, 3495 (1998).
[7] F. Piazza and L. Pavesi, Phys. Rev. B **47**, 4644 (1992).
[8] W. Müller, H. T. Grahn, R. J. Haug, and K. Ploog, Phys. Rev. B **46**, 9800 (1992).
[9] F. Claro, J. F. Weisz, W. Müller, K. v. Klitzing, H. T. Grahn, and K. Ploog, Phys. Rev. B **53**, 7970 (1996).
[10] T. Schmidt, A. G. M. Jansen, R. J. Haug, K. von Klitzing, and K. Eberl, Phys. Rev. Lett. **81**, 3928 (1998).
[11] J. F. Palmier, A. Sibille, G. Etemadi, A. Celeste, and J. C. Portal, Solid State Commun. **7**, B283 (1992).
[12] D. Miller and B. Laikhtman, Phys. Rev. B **52**, 12 191 (1995).
[13] E. Economou, *Green's Functions in Quantum Physics* (Springer Verlag, Berlin, Heidelberg, New York, Tokyo, 1983).
[14] A. Wacker and B. Y.-K. Hu, Phys. Rev. B **60**, 16 039 (1999).
[15] R. d. L. Kronig and W. G. Penney, Proc. R. Soc. London, Ser. A **130**, 499 (1931).
[16] S. Datta, *Electronic Transport in Mesoscopic Systems* (Cambridge University Press, Cambridge, 1995).
[17] D. K. Ferry and S. M. Goodnick, *Transport in Nanostructures* (Cambridge University Press, Cambridge, 1997).
[18] A. Wacker, S. Bose, C. Rauch, G. Strasser, and E. Gornik, Superlattices Microstruct. **25**, 43 (1999).
[19] R. Peierls, Z. Phys. **80**, 763 (1933).
[20] D. S. Fisher and P. A. Lee, Phys. Rev. B **23**, 6851 (1981).
[21] H. U. Baranger and A. D. Stone, Phys. Rev. B **40**, 8169 (1989).